

RESEARCH

Open Access



# Multi-orientation local ternary pattern-based feature extraction for forensic dentistry

Karunya Rajmohan<sup>1\*</sup> and Askarunisa Abdul Khader<sup>2</sup>

\*Correspondence:  
karu.aug19@gmail.com  
<sup>1</sup> Computer Science  
and Engineering, Vickram  
College of Engineering,  
Enathi, Tamilnadu 630561,  
India  
Full list of author information  
is available at the end of the  
article

## Abstract

Accurate and automated identification of the deceased victims with dental radiographs plays a significant role in forensic dentistry. The image processing techniques such as segmentation and feature extraction play a crucial role in image retrieval in accordance with the matching image. The raw image undergoes segmentation, feature extraction and distance-based image retrieval. The ultimate goal of the proposed work is the automated quality enhancement of the image by providing advanced enhancement techniques, segmentation techniques, feature extraction, and matching techniques. In this paper, multi-orientation local ternary pattern-based feature extraction is proposed for feature extraction. The grey level difference method (GLDM) is adopted to extract the texture and shape features that are considered for better results. The image retrieval is done by the computation of similarity score using distances such as Manhattan, Euclidean, vector cosine angle, and histogram intersection distance to obtain the optimal match from the database. The manually picked dataset of 200 images is considered for performance analysis. By extracting both the shape features and texture features, the proposed approach achieved maximum accuracy, precision, recall, F-measure, sensitivity, and specificity and lower false-positive and negative values.

**Keywords:** Forensic dentistry, Fuzzy rule-based probability, Local texture orientation ternary pattern extraction, Neumann boundary detection, Distance-based image retrieval

## 1 Introduction

Forensic dentistry facilitates the identification of a deceased person using both the ante-mortem and post-mortem dental images [1]. In a crime or natural calamity, proving the physical identity becomes a challenging task with the remains of a disguised body. Though the DNA and fingerprints are utilized to establish the identity of a person, forensic dentistry plays a better role because the dental remains are durable than the other parts and hence it lasts for a long time [2]. Despite durability, the dental forensics is more crucial than fingerprints and iris as the shape of teeth may vary due to the aging factor. The dental records obtained after post-mortem are in the form of radiograph images, panoramic images, bitewing images, or periapical images [3]. The images are compared and identified by the general image processing steps that include preprocessing, image enhancement, image segmentation, feature extraction, and classification [4].

The features such as the contour of the teeth crown shape, missing tooth, bridges, and distance between the teeth are considered during victim identification. In Dental Biometrics, the information about the tooth, such as contours, shape and size of the dental works, relative positions of neighboring teeth and distance between the neighboring dental works are also considered [5–9].

Identity of an individual is confirmed by the dentist in accordance with the number of matching features. The manual identification requires the preparation of the charts for each individual based on the features listed which is a complex task for medical professionals. The automated process can compare the records of multiple individuals at a time in the case of a large dataset. Feature extraction and matching are considered as the key steps in automation of the forensic dentistry applications.

In the feature extraction step, the prominent features including prosthesis, contour, and crown shape are extracted from the radiographic dental images. The segmentation of images and contour extraction are two important steps in the extraction of appropriate features. In general, the segmentation is performed by the common edge detection algorithms that fail in eliminating noise and corrupted pixels from the raw radiographic images. The segmentation involves gap valley detection and tooth isolation. In this paper, Neumann boundary-based segmentation algorithm is proposed to derive the region of interest (ROI). The radiographic segmentation includes fuzzy rule-based probability for gap valley detection of the teeth. In feature extraction, both the texture and shape features are considered along with the proposed multilevel orientation local ternary pattern extraction algorithm. The texture features are extracted by the application of the grey level difference method (GLDM) that helps in the effective extraction of essential features. The segmentation and feature extraction methods are not enough to identify a human from a large set of data. To have an accurate match, images are retrieved based on similarity scores computed between the query image and the images in post-mortem dentistry records. The similarity scores are computed using four different distance formulae, namely, Euclidean distance, vector cosine angle distance, Manhattan distance and, histogram intersection distance. Finally, the distance measures are applied to the image retrieval process to identify appropriate distance that suits for content-based image retrieval of dental images.

The Manhattan and Euclidean distance-based similarity score retrieves better match of the images. The distance-based retrieval is carried out separately using local ternary pattern features, shape features, and the combination of texture and shape features. The local ternary pattern is highly robust to the noise and high discrimination capability for the accurate extraction of the shape and texture features. The main objectives of the research work are:

1. To extract the texture and shape features for optimal retrieval of images by using multi-orientation local ternary pattern-based feature extraction algorithm.
2. To retrieve the better matching of the images based on the distance-based similarity score.

From the experimental analysis, it is observed that the accuracy, precision, recall, and F-measure of the proposed method is below 80%, specificity and sensitivity is 80%, with the extraction of the shape feature only. By extracting both the shape features and texture features, the accuracy, precision, recall, F-measure, sensitivity, and specificity are above 90%. Hence, the contours of both the ante-mortem and post-mortem radiographs are optimized by using both the shape and texture features. The most significant criterion is to identify the distance between the radiographs. To have an accurate match, images are retrieved based on the similarity scores computed between the query image and the images in the post-mortem dentistry records. The similarity of both radiographs is measured based on the distance evaluation. The Manhattan and Euclidean distance provided better matching results than the vector cosine angle distance and histogram intersection distance.

The paper is organized as follows: Sect. 2 reviews the previous researches on dental radiograph images and the segmentation, feature extraction, image retrieval techniques. Section 3 explains the proposed research methodology including segmentation, feature extraction, and matching. Section 4 describes the experimental setup and Sect. 5 presents the performance evaluation results. Section 6 concludes the work with the advantages, drawbacks and scope for future enhancement.

## 2 Literature review

This section reviews the state-of-the-art approaches for image segmentation, feature extraction, and image retrieval techniques applied in dental radiographic images. The tooth problems are efficiently diagnosed by segmenting the radiograph images of teeth. The noise removal and pixel correction is done by the application of the smoothing filter. Otsu's thresholding technique is suggested to segment the dental images and the region of interest is extracted by component analysis. The processed images are enhanced using CLAHE based on histogram which improves the segmentation of images [1]. The tooth displacement is detected using the 3D models and color images which is one of the critical tasks in the dental field. The extraction of location and shape information of the teeth is performed using instance segmentation. The instance from the teeth images is segmented using a novel object contour refinement technique. The images are captured from the mobile and the dataset is trained with the assistance of Mask Recurrent Convolutional Neural Networks (R-CNN) [2].

The isophote characteristics are considered for the identification and extraction of the cystic region from the dental images. The extraction is done with the application of the fast marching method that works based on the Dijkstra's algorithm. The shortest distance from the seed, found out by using the maximum iso-center, is used to extract the boundary of the cyst area. Each point is traversed not more than one time to minimize time consumption and make the process fast [3]. An active contour model is applied to segment the dental images through the efficient extraction of the region of interest. In general, edge detection algorithms are applied to extract regions of interest but the accuracy is not well defined, which can be resolved by the snake-based approach. The snake-based approach used in the paper segregates the original image into several sub-images in such a way that it satisfies the appropriate conditions [4].

The morphological operators are applied to enhance and segment the dental images that are not clear in radiography. The manual method of converting an image to grey level, clipping, and cropping of the cyst areas are compared with the ground truth images are performed. The morphological operations the image greatly facilitates visualization which in turn helps the practitioners to diagnose effectively [10]. In the segmentation process, the challenges tasks include the problem of fixing the initial contour and the weak image boundaries. The complex geometries in the radiographic dental images can be resolved using the level method thereby identifying the exact location. The boundary leakage problem is also eliminated on the application of the level method [11]. The morphological operation is integrated with sparse representation classifiers to extract the hard tissues from dental images. The local illumination in an image is imbalanced which causes the corrupted pixels and noise in an image. The imbalance illumination issue is resolved by preprocessing the images. The optimized marker region on the image is considered in the extraction of hard tissue using the watershed transform [12].

Principal component analysis (PCA) and Discrete Wavelet Transform (DWT) are integrated to extract the features from the oral images. The Support Vector Machine (SVM) classifier is used to classify the gender of the persons, based on teeth. This method of gender classification is rapid and cost-effective with minimum effort [13]. The radiograph images are enhanced to detect the infected tooth through cluster-based self-organizing maps. Similar patterns of the infected teeth are extracted to make the diagnosis effective. The Gaussian filter is applied in the image from which the features are extracted for further processing [14]. The caries in the dental radiographic images are detected using texture-based feature extraction method along with a multiclass SVM classifier. The region of interest is identified using the K-means clustering method used for segmentation. The grey level co-occurrence matrix is utilized to extract the texture features of an image. These texture-based features resulted in the exact measurements of the teeth [15]. The diagnosis of dental caries is carried out based on texture features to attain better results. The images are sharpened using Laplacian filter and it is subjected to morphological operations along with adaptive thresholding for segmentation.

An integration of grey level co-occurrence matrix and grey level difference method is performed to extract the texture features of the teeth [16].

The query images are retrieved based on the discriminative features of an image. The texture features are extracted using the local binary pattern (LBP) method which is modified in such a way that it utilized the four most significant bits of the radiographic image. The Euclidean and Manhattan distances are applied to estimate the similarity between the query image and the images available in the dataset [17]. The humans are recognized using the missing tooth and artificial teeth from the X-ray images. The processes utilized the shape and texture features for effective identification in a rapid manner. The shape features are extracted using a mathematical tooth approximation technique that outperformed the region-based contour model [18]. The Tamura and color features are combined for retrieving the dental images from the database using the content-based image retrieval technique. Various levels of the images are identified using different features including color moments, histogram and texture. The similarity score between the images plays a vital role in the content-based retrieval system, which is computed using various distance measures [19]. Pushparaj, Gurunathan, and Arumugam [20] proposed skeleton-based measures and contour-based techniques for shape matching in dental radiographs and photographs. Due to better shape matching based on the skeleton measures, automated dental identification is achieved with high precision and recall.

### **3 Proposed methodology**

#### **3.1 Dental image segmentation**

The dental image consists of both maxillary and mandibular teeth which make the identification process critical. Hence, the radiographic images are segmented to have a single tooth in each segmented block, which in turn facilitates the detection of ROI for every tooth. Initially, the teeth are segmented row-wise that is lower jaw and upper jaw teeth in each row. Further, each row is segmented to isolate each tooth from the neighboring teeth. The segmentation includes two basic steps such as gap valley detection and tooth isolation as follows.

##### **3.1.1 Gap valley detection**

The gap valley can be identified based on the variation in the intensity of both lower and upper jaw images. The pixel intensity values in the 'X' axis are summed up together to measure the grey level values. The teeth portion of the images has a higher grey level value which helps in differentiating it from the tissues in the jaws. While projecting a histogram representation of the grey level values of the image, a valley that represents the gap of the upper and lower teeth is generated. The fuzzy rule-based probability is proposed to identify the gap valleys, as there may be many projections in the histogram which look like gap valleys. The enhanced image is transformed as a masked image through which a gap valley can be detected. The linear image is converted into subscripts on which the Gaussian distribution probability is applied.

---

**Fuzzy rule based probability**

---

**Input:** Enhanced Image  $E_{img}$ **Output:** Gap valley detected mask  $G_{img}$ 

---

**Step 1:** Convert linear image into subscripts**Step 2:** Apply Gaussian distribution probability

$$P(g_d) = \frac{1}{\sqrt{2\pi\sigma^2}} e^{-\frac{(c_x - \mu)^2}{2\sigma^2}}$$

**Step 3:** Compute the random indices of the pixels

$$u = E_{img}(rand_{ind})$$

**Step 4:** Compute the standard deviation of gap valley mask image

$$v = std(E_{img})$$

**Step 5:** Initialize the weight matrix

$$w = ones(dim(E_{img}))$$

**Step 6:** Initialize the updated vectors and compute the probability

$$u_0 = 0; v_0 = 0; w_0 = 0$$

$$prob = \sum (u - u_0)^2 + \sum (v - v_0)^2 + \sum (w - w_0)^2$$

$$prob = (\sqrt{2\pi} * v(i))^{dim} * \exp, \text{ if } prob(i) > 10^{-6}$$

**Step 7:** The random indices and the standard deviation is updated by multiplying the probability value with the pixel values of enhanced image.

$$u = prob.*E_{img}$$

$$v = \sqrt{\frac{1}{dim * (prob.*E_{img})}}$$

Step 8: Mask can be obtained by,

$$k = u(:, 1:3)$$

$$G_{img}(:, i) = \lim_{i \rightarrow 1}^n v(:, 1) * k * E_{img}(:, i)$$

Where n - number of columns in the image

Fuzzy rule designed,

$$G_{img}(ii) = \lim_{ii \rightarrow 1}^n \begin{cases} 1; & \text{if } ii \geq n/4 \ \& \ ii < n/2 \\ 0; & \text{else} \end{cases}$$


---

The histogram consists of 'n' number of valleys among which one of them is the gap valley which is identified based on the probability computed using Gaussian distributed probability as shown in Eq. (1)

$$P(g_d) = \frac{1}{\sqrt{2\pi\sigma^2}} e^{-\frac{(c_x - \mu)^2}{2\sigma^2}}, \quad (1)$$

where  $\sigma$  is the standard deviation,  $\mu$  is the mean value of all the pixels and  $c$  is the continuous variable that range from  $-\infty$  to  $+\infty$ . The gap valleys will have lower intensity values that can be stated as the lower intensities will have a higher probability of being a gap valley. The jawbones will have higher intensity values hence it is a hard tissue. The probability of gap valley is computed using the equation given in Step 6 of the fuzzy rule-based probability algorithm. The values initialized manually will lead to a certain error that is computed by finding the standard deviation. The probability of gap valley is less in the case of a large error value. The images are vertically segregated if the gap of the jaws does not lie parallel to the  $x$ -axis. The vertical partitioning also resolves the issue of inhomogeneous intensities in X-ray. The Gaussian masked image is obtained by the application of fuzzy-based probability. The column pixels are assigned as value '1' in case of  $ii \geq n/4$  and  $ii < n/2$ , otherwise marked as '0'.

### 3.1.2 Tooth isolation

The upper and lower jaw segregation procedure is followed for tooth isolation which is done by drawing a boundary line on the row of the teeth. The upper and lower jaws are differentiated according to the intensity values. The intensity values of each column in an image is summed up together in a vertical axis from top to bottom and bottom to top until a gap valley is reached. The gap valleys are formed on the gap between each tooth using which the segmentation is carried out. If the sum of intensity values is found to be less than the threshold value there is a high probability of a gap between the neighboring teeth. The procedure of adding intensity values and comparing it with the threshold value should be repeated for all the teeth in the upper and lower jaw. The segmentation relies based on the image quality where the poor quality of the image may lead to over or under segmentation. The under and over-segmentation is resolved by adding and deleting pixels, respectively. The ROI for every tooth is identified based on the segmented output. The center point of the rectangular area of ROI is considered as the center of the crown which is further utilized for shape feature extraction.

### 3.2 Crown extraction

The region of teeth above the jaw is called as crown of the teeth and the invisible portion below the jaw is known as the root of the teeth. The ROI identified during segmentation is segregated into two vertical halves with the center of the crown as a base. The pixels are categorized as tooth pixels and background pixels. The crown center is the seed point that differentiates both the crown and root area of the teeth. The energy term is computed using the Bernoulli Naïve Bayes probability from the seed point. The conditions for boundary predictions are set using the Neumann boundary condition. The new energy is estimated based on the neighborhood pixels and compared with the old energy, which gives the deviation probability. The contour for the crown of the teeth is outlined with the enlarged region. The basic expression for this boundary detection is given as:

$$\frac{\partial \vartheta}{\partial t} = |\nabla \vartheta| \operatorname{div} \left( \frac{\nabla \vartheta}{|\nabla \vartheta|} \right). \quad (2)$$

Here,  $\frac{\nabla \vartheta}{|\nabla \vartheta|}$  represents the unit normal to a boundary of  $\varepsilon$  at each seed point and  $\text{div}\left(\frac{\nabla \vartheta}{|\nabla \vartheta|}\right)$  represents the curvature of a Neumann boundary.  $\varepsilon$  indicates the quasi-isometry.

Initially, the histogram for each gap valley detected image is computed and the parameters are initialized for the estimation of Bernoulli naive Bayes probability, which in turn identifies the ROI. Depending upon the conditional Bernoulli event model, the distance value and the detection probability can be calculated by the following equation:

$$d = M(k) - I_{\text{gap}}(\cdot), \tag{3}$$

$$\text{Prob} = \prod_{k=1}^n \tau_k^{\vartheta(k)} (1 - d)^{\vartheta(k)}, \tag{4}$$

where  $\tau$  is the distribution function initial parameter and  $k$  is the number of potential pixels present in the segmented region surface.

The Neumann boundary condition is updated as shown in equation (\*),

$$\text{NB} = -k \frac{d\text{Prob}(0, t)}{dx}. \tag{5}$$

Then the Neumann boundary condition can be obtained as a mask region. During each iteration, the index, curvature and energy values are updated. Let the index of the mask region is  $\text{id} = \text{loc}(\text{NB})$ .

The curvature is calculated using,

$$\text{Curvature}, \frac{\partial c}{\partial t} = \nabla c \text{NB}(\text{id}) + n, \tag{6}$$

where  $n$ : constant.

$\nabla c$ : pixel difference at 8-Different direction in angles of  $0^\circ, 30^\circ, 45^\circ, 60^\circ, 90^\circ, 120^\circ, 135^\circ, 180^\circ$  and the related opposite angles.

The internal and external energy updation are given as:

$$\text{Energy}_{\text{in}} = \lim_{i \rightarrow 1tom} \left\{ \begin{array}{ll} \text{NB}(i) & \text{if}(\text{NB}(i) \leq 0) \\ 0 & \text{else} \end{array} \right\}, \tag{7}$$

$$\text{Energy}_{\text{ext}} = \lim_{i \rightarrow 1tom} \left\{ \begin{array}{ll} \text{NB} & \text{if}(\text{NB}(i) > 0) \\ 0 & \text{else} \end{array} \right\}, \tag{8}$$

where  $m$  is the size of the image. Thus, the total energy can be estimated as:

$$\text{Energy}, E = \frac{(I_{\text{gap}}(\text{id}) + \sum \text{Energy}_{\text{in}})}{\max((I_{\text{gap}}(\text{id}) + \sum \text{Energy}_{\text{ext}}))} + \alpha * \frac{\partial c}{\partial t}. \tag{9}$$

The difference of energy updation with respect to time is given by:



$$dt = \frac{t}{\max(E)}, \quad (10)$$

where  $t$  represents the time period. The direction is updated as follows:

$$D_{\text{Pos}} = \sqrt{\max(\text{Pos}_B^2, \text{Neg}_F^2) + \max(\text{Pos}_R^2, \text{Neg}_L^2)}, \quad (11)$$

$$D_{\text{Neg}} = \sqrt{\max(\text{Neg}_B^2, \text{Pos}_F^2) + \max(\text{Neg}_R^2, \text{Pos}_L^2)}, \quad (12)$$

where  $\text{Pos}_B, \text{Neg}_B, \text{Pos}_F, \text{Neg}_F, \text{Pos}_R, \text{Neg}_R, \text{Pos}_L, \text{Neg}_L$ —positive and negative position of backward, forward, right and left, respectively.

The contour weight updation is determined by:

$$Wt_{i+1} = Wt_i - dt * \frac{Wt_i}{20 * \sqrt{Wt_i^2 + 1}} * (NB + dt * E), \quad (13)$$

where  $Wt_i$  is the segmented contour template path for  $I=1$  to iteration level and  $dt$  is the energy updation difference.

### 3.3 Feature extraction

The texture and shape features are extracted to detect the ROI from the segmented images. The texture and visual properties including brightness, regularity, and coarseness are required for effective pattern matching. The multi-orientation based local ternary pattern algorithm is proposed to extract the texture features along with the grey level difference method (GLDM). The shape features including area, perimeter, and equivalent diameter are estimated for the segmented region. The quantitative measurements are obtained by manipulating the images using mathematical techniques.

### 3.4 Multi-orientation local ternary pattern-based feature extraction

The images are converted into patterns using multi-orientation local ternary pattern-based feature extraction by comparing the neighboring pixels with the center pixels of the image. The pixel similarity is computed using the local ternary pattern in which the slightly varied pixels are grouped. The texture patterns are extracted using the local ternary pattern through multiple orientations in a  $3 \times 3$  matrix. It facilitates the identification of macro features under the grey-scale transformation of an image. The neighboring pixels undergo thresholding with the center pixel value which results in a binary code for each pixel. The binary pattern turns out to be '1' if the neighbor pixel value  $\text{SegI}(i, j)$  and the center pixel  $I_c$  are greater than the computed pattern  $S_k$ . The characteristics of the images such as curved edges, heap, and flat areas, and spots are identified from the generated binary patterns. The neighboring pixels in a specific ROI are interpolated with equal space. For each pixel in an image, 8 neighboring pixel values are considered to estimate the similarity score and to compare with the threshold value. The local ternary pattern operators are applied at different levels and the final output is the combination of different orientations.

---

**Multi Orientation Local Ternary Pattern based Feature Extraction**

---

**Input:** Segmented Result SegI

**Output:** Extracted pattern features  $F_{lotp}$

---

**Step 1:** Perform the feature extraction for SegI

$$[x \ y] = \text{size}(\text{SegI})$$

$$P_t = \lim_{i \rightarrow 2 \text{ to } x-1} \lim_{j \rightarrow 2 \text{ to } y-1} \text{SegI}(i-1:i+1, j-1:j+1)$$

**Step 2:** Compute nearest patterns for the center pixel

$$S_k = \lim_{k \rightarrow 1 \text{ to } 8} \begin{cases} P_{t_{1+\text{mod}(k+5,7)}}, P_{t_{1+\text{mod}(k+6,9)}}, P_{t_{k+1}}, P_{t_{\text{mod}(k+2,8)}} & \text{if } k == \text{odd} \\ P_{t_{k-1}}, P_{t_{\text{mod}(k+1,8)}} & \text{else} \end{cases}$$

**Step 3:** Estimate binary pattern,

$$B_{P_t}^1(k) = \begin{cases} 1; & \text{if } S_k \geq \text{SegI}(i, j) \\ 0 & \text{else} \end{cases}$$

SegI(i, j) –It’s should be a nearest pixel

$$B_{P_t}^2(k) = \begin{cases} 1; & \text{if } S_k \geq I_c \\ 0; & \text{else} \end{cases}$$

$I_c$  –Center Pixel

$$R_i(k) = \begin{cases} 0; & \text{If } B_{P_t}^1(k) == 0 \ B_{P_t}^2(k) = 0 \\ 0; & \text{elseif } B_{P_t}^1(k) == 1 \ B_{P_t}^2(k) = 1 \\ 1; & \text{else} \end{cases}$$

$$P_t^{\text{final}}(k) = \begin{cases} 1; & \text{If } \dim(R_i == 1) \geq \left(\frac{\dim(S_k)}{2}\right) \\ 0; & \text{else} \end{cases}$$

**Step 4:** Compute final ternary pattern,

$$\text{Features} = \lim_{i \rightarrow 1 \text{ to } \dim(P_t^{\text{final}})} P_t^{\text{final}} + (P_t^{\text{final}} * 2^{i-1})$$


---

**3.4.1 Grey level difference method**

The image points are geometrically related for measuring the texture features from the joint gray level histogram of the image. The grey level co-occurrence matrix and grey level difference method are similar to each other. The probability density function of the grey levels is utilized to obtain the texture features. The original image  $I(x, y)$  is subtracted from which the probability density function is computed.

The subtracted image is defined as follows:

$$\text{sub}(p, q) = |f(p, q) - f(p + dx, q + dy)|, \tag{14}$$

where  $dx$  and  $dy$  are the integer values.

The probability density function obtained from the subtracted images are given below:

$$\text{pdf}(i, d) = \text{PDF}(\text{sub}(p, q) = i). \quad (15)$$

The rotational textures are derived from the horizontal and vertical directions as well as from  $0^\circ$ ,  $45^\circ$ ,  $90^\circ$  and  $135^\circ$ .

### 3.5 Image retrieval

An ante-mortem query image is provided to retrieve an exact match of the post-mortem image. The query image undergoes segmentation and feature extraction to optimize the contours of both images. The vital criterion is to identify the distance between the ante-mortem and post-mortem radiographs.

#### 3.5.1 Distance matching

According to the number of teeth in the query image, its sub-images are generated from the database, which are same as the number of teeth. A feature vector  $F = \{x_1, x_2, \dots, x_n\}$  is generated by considering the  $n$ -dimensions of the image. This facilitates in identifying the similarity of two images and the order of images according to their distance. The closest match of a query image can be easily perceived by comparing images with the four distances namely, Euclidean distance, vector cosine angle distance, Manhattan distance, and histogram intersection distance.

**3.5.1.1 Euclidean distance** The distance between two points  $X(m_1, n_1)$  and  $Y(m_2, n_2)$  using Euclidean distance can be measured as follows:

$$E(X, Y) = \sqrt{(m_1 - m_2)^2 + (n_1 - n_2)^2}. \quad (16)$$

The Euclidean distance in an  $n$ -dimensional points that is  $X(m_1, m_2, \dots, m_n)$  and  $Y(n_1, n_2, \dots, n_n)$  is modified as:

$$E(X, Y) = \sqrt{(m_1 - n_1)^2 + (m_2 - n_2)^2 + \dots + (m_n - n_n)^2}, \quad (17)$$

which can be simplified as

$$E(X, Y) = \sqrt{\sum_{i=1}^n (m_i - n_i)^2}. \quad (18)$$

**3.5.1.2 Manhattan distance** The Manhattan distance between two points  $X(m_1, n_1)$  and  $Y(m_2, n_2)$  is given as:

$$M(X, Y) = |(m_1 - m_2)| + |n_1 - n_2|. \quad (19)$$

In  $n$ -dimensional aspect, the Manhattan distance is generalized as:

$$M(X, Y) = |(m_1 - n_1)| + |m_2 - n_2| + \dots + |m_n - n_n|, \quad (20)$$

$$M(X, Y) = \sum_{i=1}^n |m_i - n_i|. \quad (21)$$

**3.5.1.3 Vector cosine angle distance** In vector cosine angle distance,  $\text{Cos}\theta$  is considered as the vector angle between two vectors  $A \equiv (a_1, a_2, \dots, a_n)$  and  $B \equiv (b_1, b_2, \dots, b_n)$ . The distance is measured as given below:

$$\text{VCA}(A, B) = \frac{\sum_i a_i b_i}{\sqrt{\sum_i (a_i)^2} \sqrt{\sum_i (b_i)^2}}. \quad (22)$$

The simplified formula for vector cosine angle distance can be given as:

$$\text{VCA}(A, B) = \frac{A \cdot B}{\|A\| \|B\|}. \quad (23)$$

The vector cosine angle distance adopts to the usage of multiple features there by combining distance between two images.

**3.5.1.4 Histogram intersection distance** The similarity between the query image and the image stored in the database computed using histogram intersection distance can be represented as:

$$\text{HI}(Q, I) = \frac{\sum_r \min(Q_r(r), I_r(r)) + \sum_g \min(Q_g(g), I_g(g)) + \sum_b \min(Q_b(b), I_b(b))}{\min(Q, I) * 3}, \quad (24)$$

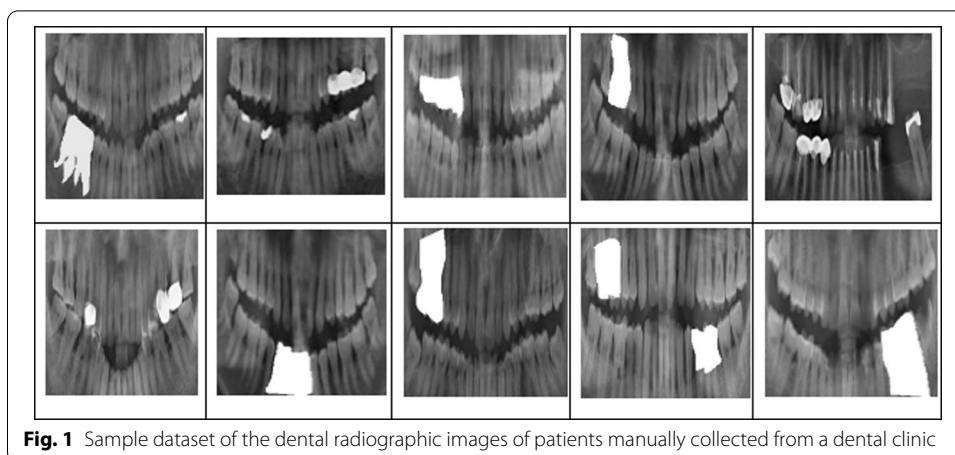
where  $I$  is the image stored in database,  $Q$  is the query image  $r, g, b$  are the primary colors red green and blue, respectively.

## 4 Experimental setup

The experimentation is performed using two datasets, Dataset A and Dataset B with ante-mortem and post-mortem images, respectively. Dataset A is manually collected from CSI College of Dental Sciences and Research, Madurai, Tamilnadu. The collected dataset from the dental clinic consists of 200 samples of radiograph images. It includes 20 samples of people with a missing tooth and 20 samples of people with dentures. The process of collecting radiographic images of dead persons is critical due to ethical reasons. The consent of the relatives of the dead person and official approval from government officials are mandatory for acquisition. Due to the difficulties in the collection of post-mortem radiographs Dataset B is constructed manually. Dataset B is generated by performing simple morphological operations on the images contained in Dataset A. The white space in the sample dataset is given in Fig. 1 shows the presence of missing teeth and dentures.

## 5 Results and discussion

The images in Table 1 show the input images of 4 samples which are enhanced further. The gap valley in the upper and lower jaws is identified. The shape features are utilized to segment the teeth. The final teeth shape is extracted using the shape and texture



features. The segmentation performance is measured in terms of accuracy, precision, recall, sensitivity, specificity.

In the segmentation results, the proposed model attained almost 98% for all the sample images. The sensitivity and specificity are around 99% and 96%, respectively. The model resulted in insignificant values of false negative and false-positive rates, thereby attaining 98% precision and 99% recall. The portion of the radiograph selected for subjects with a missing tooth is depicted in Fig. 2. Table 2 shows the analysis of victims with a missing tooth. The proposed model has achieved almost similar results as for victims with normal dental characteristics shown in Table 3. Table 4 depicts the performance of the subjects.

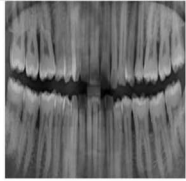
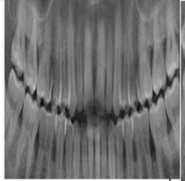
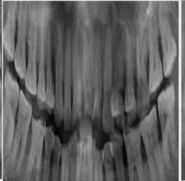

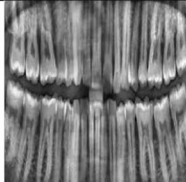
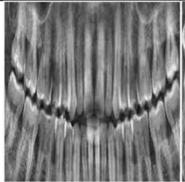
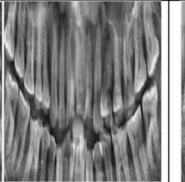
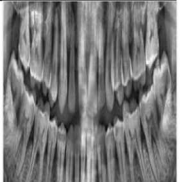
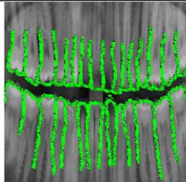
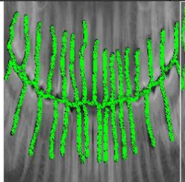
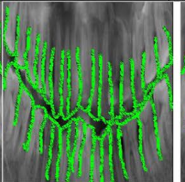
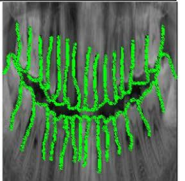
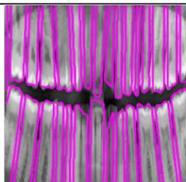
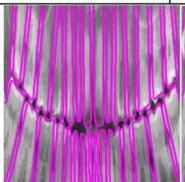
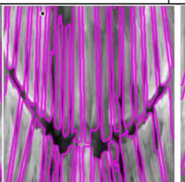
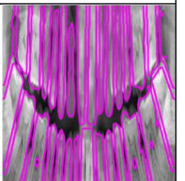
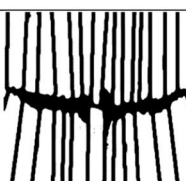
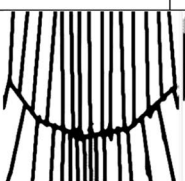
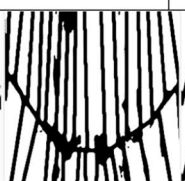
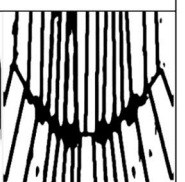

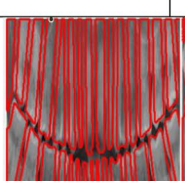
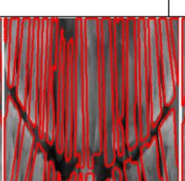
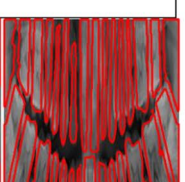
The average accuracy is about 98%, whereas specificity and sensitivity are 96% and 98%, respectively. The false-positive and false negative rates are very minimal hence resulting in 99% recall and 98% precision. The performance analysis of local ternary pattern, shape features, and texture features is shown in Figs. 3, 4 and 5, respectively. The Manhattan distance, Euclidean distance, vector cosine angle distance and histogram intersection distance are utilized to retrieve the images from the database. The accuracy, precision, sensitivity, recall, specificity, and F-measure are considered to evaluate the image retrieval.

For the features extracted using the local ternary pattern, the Manhattan and Euclidean distance provided better results when compared to vector cosine angle distance and histogram intersection distance. The image retrieved only using shape features hinders the performance, whereas the shape features along with texture features resulted in better accuracy. The Manhattan and Euclidean distance provided an optimal match to the query image.

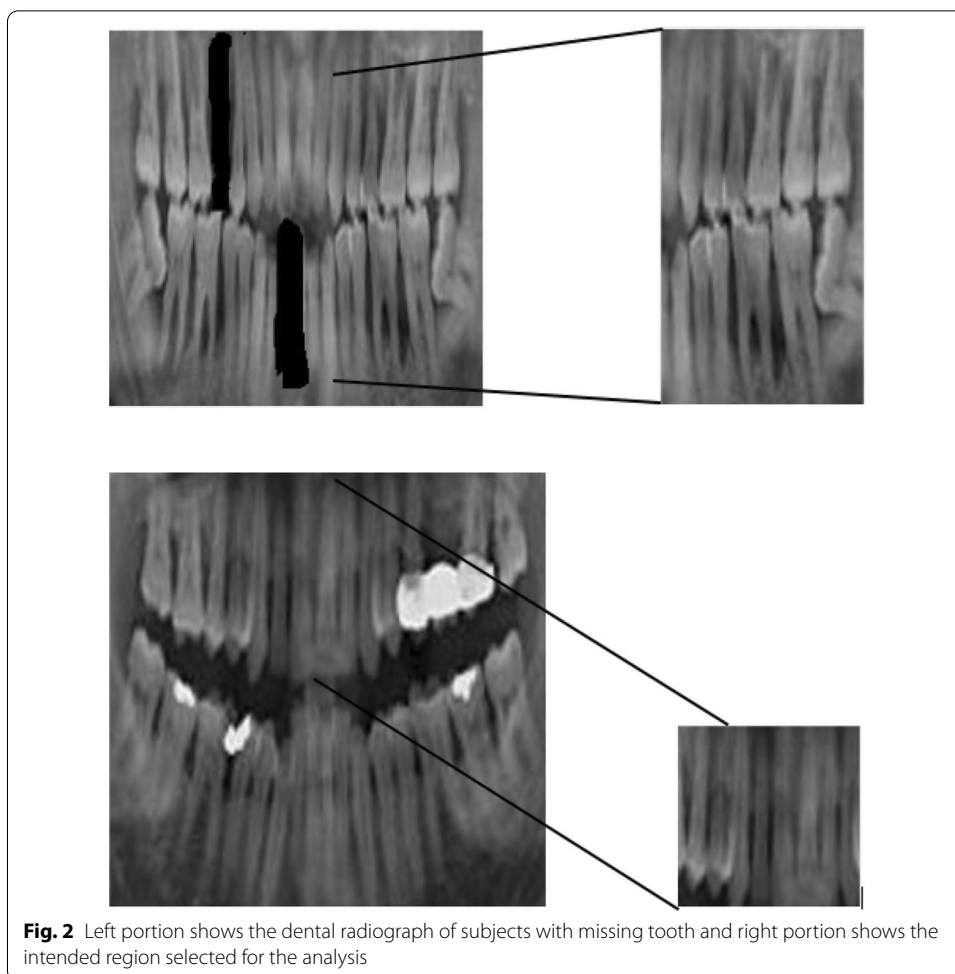
## 6 Conclusion and future work

In this paper, the process of human identification using forensic dentistry is automated using image processing techniques which has segmentation, feature extraction, and image retrieval as three major steps. The fuzzy rule-based probability algorithm is used for gap valley detection and the ROI is obtained using Neumann boundary-based Bernoulli Naïve Bayes probability. The multi-orientation local ternary pattern-based feature

**Table 1** Sample results of 4 patients from the dataset

Person	Subject 1	Subject 2	Subject 3	Subject 4
Input Image				
Enhanced Image				
Gap Valley & Tooth Isolation				
Teeth Shape Iterative Process				
Binary Segmented Result				
Final Teeth Shape Extracted				

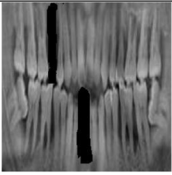
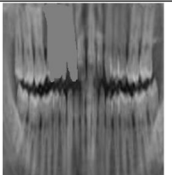
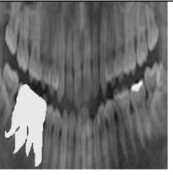
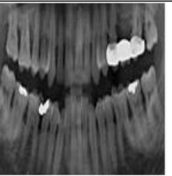
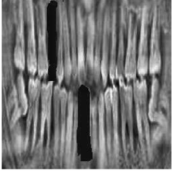
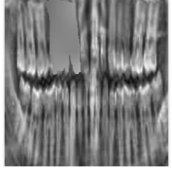

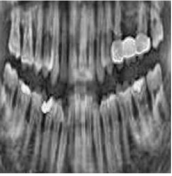
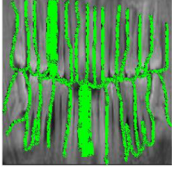
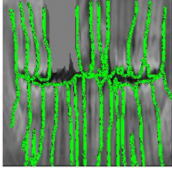
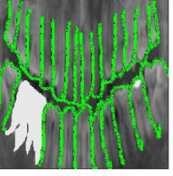
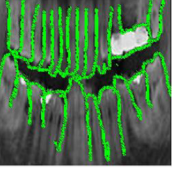
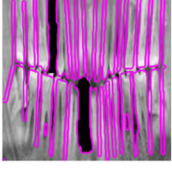
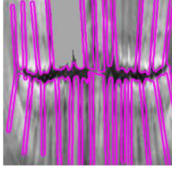
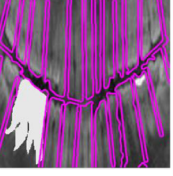
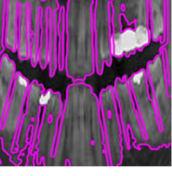

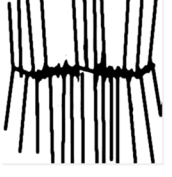
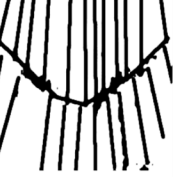

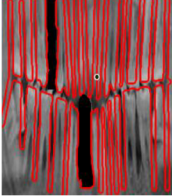
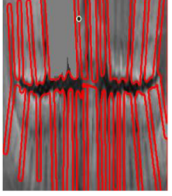


extraction algorithm is proposed to extract the features that are then integrated with the texture and shape features for optimal retrieval of images. The Manhattan and Euclidean distance-based similarity score retrieves better match of the images. The distance-based retrieval is carried out separately using local ternary pattern features, shape features, and the combination of both texture and shape features. The integrated approach has



**Fig. 2** Left portion shows the dental radiograph of subjects with missing tooth and right portion shows the intended region selected for the analysis

significant advantages in terms of accuracy, precision, recall, specificity, and sensitivity. From the experimental analysis, it is observed that the average accuracy and precision for eight test subjects is 98%, whereas specificity and sensitivity are 96% and 99%, respectively. The false-positive and negative values are very low. With the usage of Manhattan distance-based similarity metrics, the proposed approach yields maximum accuracy of 98.4%, when compared with the histogram intersection distance, Euclidean and vector cosine angle distance. In addition, the proposed strategy can be applied to a living person who requires identification. However, the local ternary patterns are not invariant under the grey-scale transform of the intensity values due to its encoding nature based on fixed predefined thresholding. The drawback of the GLCM is its limited capability of capturing the texture information at multiple scales. To overcome this limitation, in future, deep learning methods are used to automatically identify an individual from the PM/AM dental radiographs and to precisely differentiate the valid matches from the non-matches in the PM/AM dental radiographs.

**Table 2** Sample results of 4 subjects with missing tooth

Person	Subject 5	Subject 6	Subject 7	Subject 8
Input Image				
Enhanced Image				
Gap Valley & Tooth Isolation				
Teeth Shape Iterative Process				
Binary Segmented Result				
Final Teeth Shape Extracted				

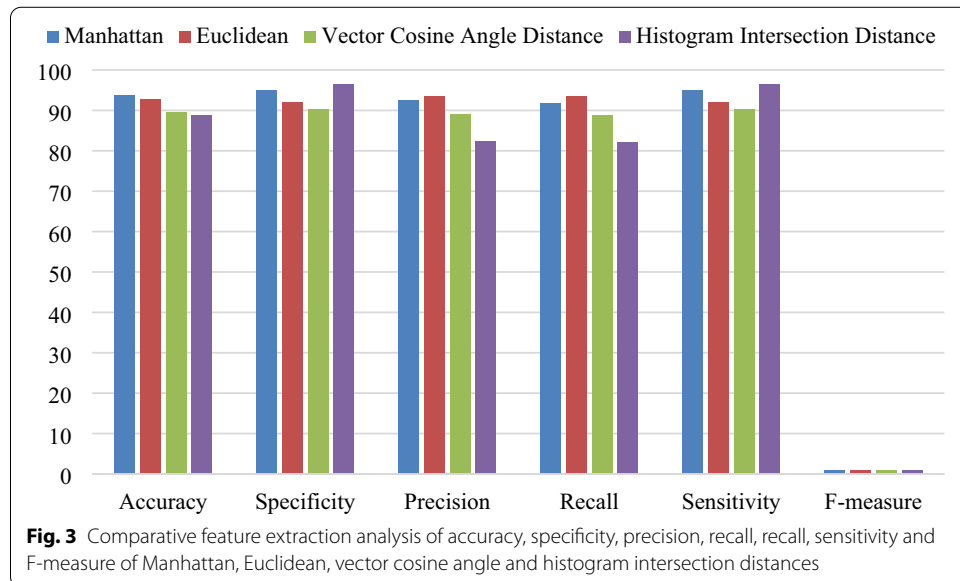


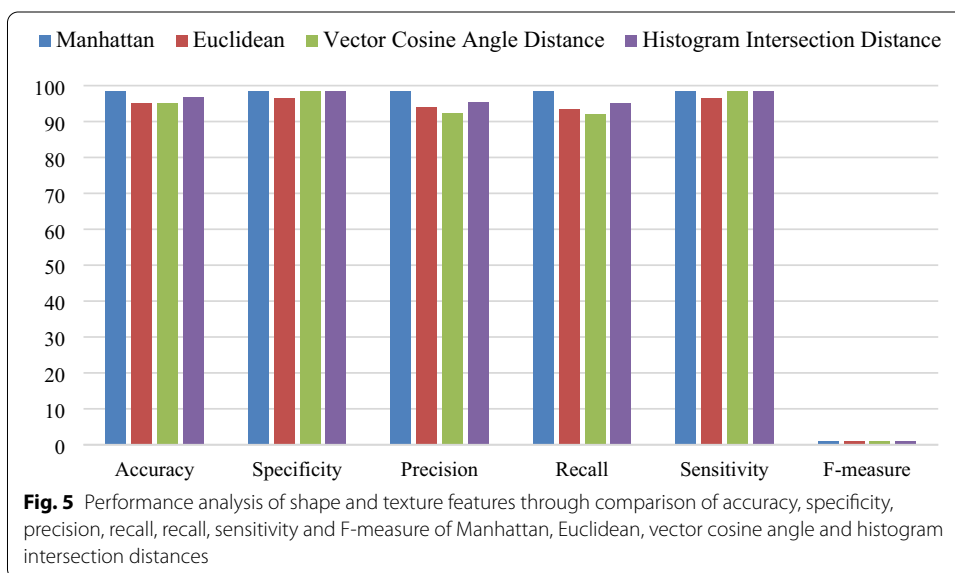
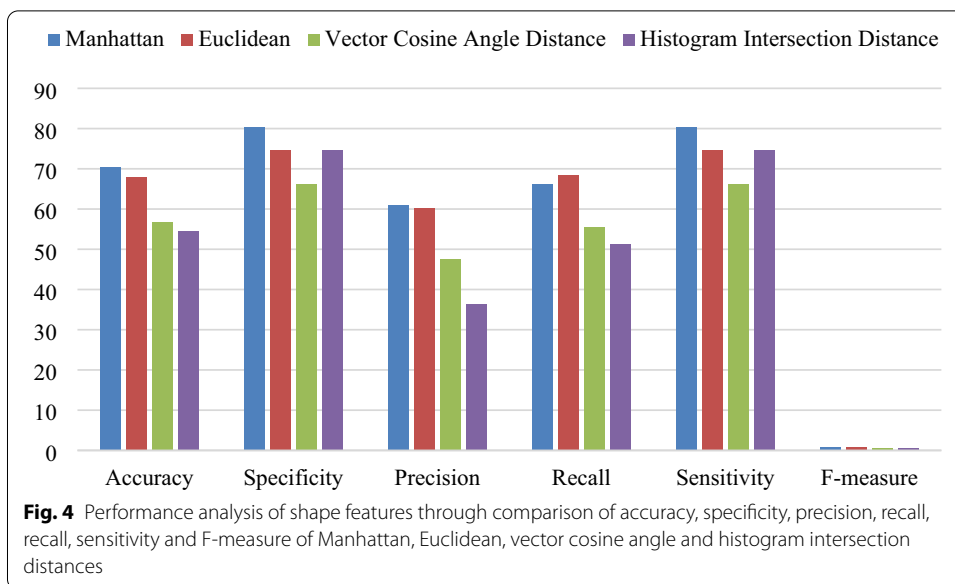
**Table 3** Performance analysis for segmentation of subjects

Person	Subject 1	Subject 2	Subject 3	Subject 4
Accuracy	98.78	98.73	98.17	98.02
Sensitivity	99.80	99.97	99.81	99.78
Specificity	96.68	95.99	95.14	94.73
Precision	98.41	98.21	97.44	97.26
Recall	99.80	99.97	99.81	99.78
False-positive rate	0.0332	0.0401	0.0486	0.0527
False-negative rate	0.0020	0.0003	0.0019	0.0022

**Table 4** Performance analysis for segmentation of subjects with missing tooth

Person	Subject 5	Subject 6	Subject 7	Subject 8
Accuracy	98.88	98.97	98.37	97.71
Sensitivity	99.90	99.93	99.75	99.53
Specificity	96.61	96.36	94.03	94.07
Precision	98.50	98.68	98.13	97.09
Recall	99.90	99.93	99.75	99.53
False-positive rate	0.0339	0.0364	0.0597	0.0593
False-negative rate	0.0009	0.0007	0.0025	0.0047





**Abbreviations**

ROI: Region on interest; GLDM: Grey level difference method.

**Acknowledgements**

The authors would like to thank the anonymous reviewers and editors for helping to improve the work.

**Author's information**

Mrs R. Karunya, working as assistant Professor in Vickram College of engineering, Enathi, Tamilnadu, has graduated her bachelor's degree in information technology (BTech IT) in 2005 and ME in Computer and communication in 2012 from Anna University, Chennai. Now she is pursuing her Ph.D. in information and communication engineering at Anna University, Chennai. Her research interest includes medical image processing, machine learning, Information Visualization, Wireless Communication and its vital applications.

Dr.A. Askarunisa working as Professor and head in KLN College of Information and Technology, Sivagangai, Tamilnadu, India. Her research interest includes Software engineering, Software testing, Image processing, Information Retrieval and video surveillance.

**Authors contributions**

Author RK participated designed the algorithm and revised the article content. RK carried out the experiments and wrote the manuscript. AA gave the suggestions on the structure of the manuscript and participated in modifying it. All authors read and approved the manuscript.

**Funding**

No funding is available.

**Availability of data and materials**

Not applicable.

**Declarations****Competing interests**

The authors declare that they have no competing interests.

**Author details**

<sup>1</sup>Computer Science and Engineering, Vickram College of Engineering, Enathi, Tamilnadu 630561, India. <sup>2</sup>Computer Science and Engineering, KLN College of Information Technology, Sivagangai, Tamilnadu, India.

Received: 25 June 2021 Accepted: 8 April 2022

Published online: 13 May 2022

**References**

1. H. Mansour, A. Fuhrmann, I. Paradowski, E.J. van Well, K. Püschel, The role of forensic medicine and forensic dentistry in estimating the chronological age of living individuals in Hamburg, Germany. *Int. J. Legal Med.* **131**(2), 593–601 (2017)
2. P. Wake, Life and death in the second person: Identification, empathy, and antipathy in the adventure gamebook. *Narrative* **24**(2), 190–210 (2016)
3. M. da Rocha Costa, F. Da Silva Filho, B.M. Lima, Contributions of forensic dentistry regarding identification methods: literature review. *Rev. Bras. Odontol* **76**, e1440 (2019)
4. R. F. Rahmat, S. Silviani, E. B. Nababan, O. S. Sitompul, R. Anugrahwati, S. Silmi, Identification of molar and premolar teeth in dental panoramic radiograph image, in. *2017 Second International Conference on Informatics and Computing (IICIC)*. (2017), IEEE, pp. 1–6.
5. H. Chen, A.K. Jain, Dental biometrics: alignment and matching of dental radiographs. *IEEE Trans. Pattern Anal. Mach. Intell.* **27**(8), 1319–1326 (2005)
6. A. Banumathi, B. Vijayakumari, A. Geetha, N. Shanmugavadivu, S. Raju, Performance analysis of various techniques applied in human identification using dental X-rays. *J. Med. Syst.* **31**(3), 210–218 (2007)
7. A.K. Jain, H. Chen, Matching of dental X-ray images for human identification. *Pattern Recogn.* **37**(7), 1519–1532 (2004)
8. M. Hofer, A. N. Marana, Dental biometrics: human identification based on dental work information, in. *XX Brazilian Symposium on Computer Graphics and Image Processing (SIBGRAPI 2007)*. (2007), IEEE, pp. 281–286.
9. O. Nomir, M. Abdel-Mottaleb, Hierarchical contour matching for dental X-ray radiographs. *Pattern Recogn.* **41**(1), 130–138 (2008)
10. V. Chandran, G. S. Nizar, P. Simon, Segmentation of dental radiograph images, in. *Proceedings of the Third International Conference on Advanced Informatics for Computing Research*, (2019). pp. 1–5.
11. T.V. Pham, Y. Lucas, S. Treuillet, L. Debraux, Object contour refinement using instance segmentation in dental images, in *International Conference on Advanced Concepts for Intelligent Vision Systems*. (Springer, 2020), pp. 99–107
12. R. KarthikaDevi, A. Banumathi, G. Ulaganathan, An automated and hybrid method for cyst segmentation in dental x-ray images. *Clust. Comput.* **22**(5), 12179–12191 (2019)
13. K.R. Jain, N. Chauhan, Segmentation of dental radiographs using active contour model, in *dental image analysis for disease diagnosis*. (Springer, Berlin, 2019), pp. 59–83
14. K.R. Jain, N. Chauhan, Enhancement and segmentation of dental radiographs using morphological operations, in *Dental image analysis for disease diagnosis*. (Springer, Berlin, 2019), pp. 39–58
15. G. Kavitha, M. Muthulakshmi, M. Latha, image segmentation using contour models: dental X-ray image segmentation and analysis, in. *Computational Techniques for Dental Image Analysis*. IGI Global, (2019), pp. 62–85.
16. B. Cheng, W. Wang, Dental hard tissue morphological segmentation with sparse representation-based classifier. *Med. Biol. Eng. Comput.* **57**(8), 1629–1643 (2019)
17. B. Uzbaş, A. Arslan, H. Kök, A.M. Acilar, Gender determination from teeth images via hybrid feature extraction method, in *The International Conference on Artificial Intelligence and Applied Mathematics in Engineering*. (Springer, 2019), pp. 446–456
18. K. Lakhani, V. Vashisht, N. Gugnani, A novel method using SOM for recognizing patterns in dental radiographs—a conceptual approach. *Informat Med Unlock.* **16**, 100236 (2019)
19. J. Premkumar, B.J. Janney, A. Nanda, S. Divakaran, P. Lavanya, Detection of caries in dental X ray images using Multi-class SVM. *J. Pharm. Sci. Res.* **11**(9), 3264–3268 (2019)
20. V. Pushparaj, U. Gurunathan, B. Arumugam, Dental radiographs and photographs in human forensic identification. *IET biometrics* **2**(2), 56–63 (2013)

**Publisher's Note**

Springer Nature remains neutral with regard to jurisdictional claims in published maps and institutional affiliations.